Available online at www.sciencedirect.com

SciVerse ScienceDirect

Journal of the European Ceramic Society 32 (2012) 547–557

www.elsevier.com/locate/jeurceramsoc

Influence of chemical and physical properties of the last generation of silicon carbide fibres on the mechanical behaviour of SiC/SiC composite

E. Buet [a,*], C. Sauder [a], S. Poissonnet [b], P. Brender [c], R. Gadiou [c], C. Vix-Guterl [c]

[a] *CEA, DEN, SRMA, Laboratoire de Technologie des Matériaux Extrêmes, F-91191 Gif-sur-Yvette, France*
[b] *CEA, DEN, SRMP, F-91191 Gif-sur-Yvette, France*
[c] *Institut de Sciences des Matériaux de Mulhouse, CNRS, LRC 7228, 15 rue Jean Starcky, 68057 Mulhouse, France*

Received 26 May 2011; received in revised form 22 September 2011; accepted 26 September 2011
Available online 22 October 2011

Abstract

SiC/SiC composites reinforced with near stoichiometric SiC ceramic fibres (Hi-Nicalon S and SA3 Tyranno fibres) are attractive materials to be used in nuclear environment. Netherless, their mechanical properties must be improved and controlled. For example, SA3 Tyranno fibres (TSA3) -reinforced composites exhibit a brittle behaviour whereas composites reinforced by Hi-Nicalon S (HNS) fibres exhibit a conventional damage tolerant response. This difference is related to the nature of the fibre/matrix (F/M) coupling. The aim of this work was to identify the SiC fibres characteristics influencing the F/M coupling and consequently the mechanical properties of the composites. The experimental results point out that the TSA3 fibres exhibit a granular and rough surface leading to an increase of the residual stress and the interfacial shear stress in the SiC/SiC composites. Beside the roughness, the experimental results also point out that the surface chemistry of the SiC fibres significantly influence the F/M bonding.

Keywords: B. Composites; B. Fibre; B. Interfaces; B. Surface; C. Mechanical properties

1. Introduction

SiC/SiC composites are commonly used for high-temperature engineering applications due to their excellent specific mechanical properties at elevated temperature. Their good microstructural stability under high-energy neutron irradiation makes them attractive to be used as blanket components in fusion or structural material in fission reactors.[1–5] Furthermore, their low permeability to fission products appears as a great advantage to avoid the reject of radioactive elements (fission products) in the heat transfer fluid. In the frame of nuclear applications, their mechanical properties remain however a drawback and must be adjusted to resist to neutronic irradiation. The mechanical behaviour of the composite depend on the fibre/matrix (F/M) bonding which is controlled by an interphase deposited on the fibre surface prior to the infiltration of the matrix in the fibre perform. The F/M-bonding must be not too strong and not too weak since its role is to deflect the matrix microcracks and hence prevent the fibres failures. Pyrocarbon is known as one of the best interphase candidate due to its crystal structure and its possibility to be strongly bonded and parallel deposited to the SiC fibres. Among the parameters influencing the mechanical properties of the composite, the nature of the C/SiC interface and/or the surface characteristics of the SiC fibres appear as predominant. The SiC surface characteristics depend on the fibres type.[13–16] The presence of oxygen and free carbon in the first generations of SiC fibres (Nicalon, Hi-Nicalon, Tyranno lox M or Tyranno ZMI) was detrimental for the mechanical properties especially when the composite was used in an oxidizing environment. To overcome this situation, new types of SiC fibres were developed in order to get a fibre with a composition as close as possible to stoichiometric SiC. In the meanwhile, the manufacturing processes of the SiC fibres were improved to decrease the surface imperfections which lead generally to premature fracture of the material.

Among this new generation, two fibre types appear as interesting to be used in SiC/SiC composites devoted to neutron irradiation: the fibres named Hi-Nicalon S and SA3 Tyranno.[6,7]

* Corresponding author. Tel.: +33 169083428.
E-mail address: emilien.buet@cea.fr (E. Buet).

0955-2219/$ – see front matter © 2011 Elsevier Ltd. All rights reserved.
doi:10.1016/j.jeurceramsoc.2011.09.023

A recent study was led on the effect of the irradiation and the temperature on the mechanical behaviour of SiC/SiC composites reinforced with Hi-Nicalon fibres.[8] It was observed that the irradiation leads to the decrease of the interfacial debond shear strength (improvement of cracking resistance) and the interfacial friction stress (improvement of damage tolerance). It is supposed that the mechanical properties of SiC/SiC composites will not be altered by an irradiation environment. Nevertheless, some of composites (TSA3 reinforced for example) stay brittle and this characteristic must be improved. This can be done through the modification and control of the F/M bond. However, a judicious optimization of the F/M bond requires first an identification of the impact of the SiC surface properties on the F/M bond. This is the objective of the present work. To progress more rapidly in this topic, we decided to use 1D model composites such as minicomposites (comprising one tow) in order to conduct several processing/characterizing iterative loops in a relatively short time as already shown in other studies.[9,10] The mechanical characteristics of composite test specimens reinforced with Hi-Nicalon S or SA3 Tyranno fibres and densified with SiC by chemical vapour infiltration were reported in a recent paper.[11] It must be noted that the SA3 Tyranno fibre is more attractive for nuclear application due to its better thermal stability.[12] Differences in the mechanical behaviour between both types of composites were observed. Especially, the SA3 Tyranno fibre reinforced composite exhibits a brittle behaviour ($\varepsilon_r < 0.3\%$) whereas the composite reinforced by Hi-Nicalon S shows a damage tolerant response ($\varepsilon_r \geq 0.5$–1%).[11] Since SiC fibres display similar mechanical characteristics (high Young's modulus and tensile strength), we assumed that the differences in the mechanical behaviour is due to the nature of the SiC/C interface related to the SiC surface properties and especially the surface roughness and surface chemistry. We present here the work performed to investigate the surface properties of the Hi-Nicalon S and SA3 Tyranno fibres in relation with the mechanical behaviour of the corresponding composite in order to identify the predominant surface characteristics responsible for the mechanical behaviour. The surface morphology, the chemical composition, the microstructure and the mechanical properties of the SiC fibres were determined using several characterization techniques. The results are discussed in order to highlight the importance of the SiC surface properties on the mechanical behaviour of the corresponding SiC/SiC composite.

2. Experimental procedure

2.1. SiC/SiC composite

SiC/SiC CVI minicomposite test specimens were prepared using Hi-Nicalon S (Nippon Carbon Co.) or SA3 Tyranno (Ube Industry Ltd.) SiC fibres. In the case of the Hi-Nicalon S (HNS) fibres, two batches were used and the samples will be referred in the text as HNS (1) and HNS (2). HNS fibres are fabricated from polycarbosilane (PCS) precursor which was crosslinked thanks an electron beam curing. These fibres are converted in ceramic at around 1000 °C and pyrolysed at higher temperature (around 1600 °C) under a H_2 atmosphere in order to get a near stoichiometric SiC fibre with a free carbon content as low as possible.

SA3 Tyranno (TSA3) fibres are produced by extruding polyaluminocarbosilane (PACS) formed by mixing polycarbosilane and a metal additive (aluminum) used as sintering aid. PACS is extruded at 220 °C to form the precusor fibre which was crosslinked in air by heating up to 180 °C. The fibres are then pyrolysed in inert gas at 1400 °C to obtain an amorphous Si–Al–C–O which was sintered in argon at 1800 °C to reach a near stoichiometric fibre.

All the fibres are sized in order to create a homogeneous and linear tow and to protect them during textile forming process. Polyvinyl acetate (PVAC) and polyethylene oxide (PEO) were used to protect the HNS and TSA3 fibres, respectively. Prior to the fibres analysis, the sizing was removed by heat treatment at 900 °C under vacuum (pressure $\sim 10^{-4}$ Pa) for 1 h. These parameters are close to the one used during the fabrication of the macroscopic CVI SiC/SiC composite.

The minicomposite test specimen is prepared as detailed elsewhere.[13] These unidirectional materials are constituted of SiC fibres, pyrocarbon interphase ($e \sim 150$ nm) and SiC matrix. The interphase and the matrix were elaborated by chemical vapor infiltration (CVI). Furthermore, TSA3 and HNS fibres were used with a 40–50% fibre volume fraction.

2.2. Characterization of the SiC fibres

The SiC fibres were characterized in terms of morphology, composition, surface roughness and surface chemistry.

The fibres diameter was measured using a Field Emission Gun Scanning Electron Microscope (FEG-SEM) Gemini 1525 from Carl Zeiss and image analysis software.

In order to investigate the microstructural properties of HNS and TSA3, X-ray diffraction (XRD) (Philips Panalytical X'PERT Pro MPD, Theta/2θ, Cu Kα radiation, $\lambda = 0.154$ nm) and Raman spectroscopy (HORIBA, laser wavelength 632.81 nm) were used directly on a group of fibre tows. The Raman spectra were recorded between 0 and 3500 cm^{-1} only on the fibre surface.

EDX analysis indicates that the samples are only constituted of C, Si, O and Al. The concentration of these elements in HNS and TSA3 fibres were determined by Inductively Coupled Plasma Atomic Emission Spectroscopy (ICP-AES). The concentration of carbon was obtained by subtracting the concentration of silicon, oxygen and aluminum from 100%. Quantitative atomic analyses were carried out using a Cameca SX 50 Electron Probe MicroAnalysis (EPMA) on polished cross-section of fibre tows. The microprobe analyses were done along the diameter of the fibre from the core to the edge (linescan measurement). The electron beam was focused on a single point with a spatial resolution of around 1 μm^3.

The surface roughness of the fibres was determined from Atomic Force Microscopy images in tapping mode (Pico LE, Molecular Imaging – SCIENTEC, lateral resolution between 0.1 nm and 10 nm). Images of 500 nm × 500 nm were taken for all samples.

X-ray Photoelectron Spectroscopy (XPS) was used to study the surface chemistry of the SiC fibres. XPS analyses were performed thanks a SCIENTA 200 X-ray photoelectron spectrometer using a concentric hemispherical analyser, an electrostatic lens with 2:1 magnification and a single channel detector. Monochromatic Al kα (1486.6 eV) operated at 420 W (acceleration tension of 14 kV, emission current of 30 mA) was used as X-ray source for all analyses. The analyzed surface area was 0.5 mm × 6 mm. A survey spectrum (0–1200 eV) was recorded in order to identify the elements present on the surface and to make a qualitative analysis. High-resolution spectra of carbon (C1s peak), oxygen (O1s peak) and silicon (Si2p peak) were recorded in the fixed analyser transmission with a pass of 30 eV after various durations of X-ray exposure, in order to demonstrate possible evolution under irradiation. Core level spectra were fitted using XPS CASA software. The XPS lineshape is represented by a symmetrical Gaussian Lorentzian product function. To finish, the component corresponding Csp2 was fitted by assymetrical model (Doniach Sunjic function) due to intrinsic loss processes such as shake-up satellites, plasmons and conduction band interactions. A Shirley background substraction was applied for all high-resolution XPS core-level spectra.

2.3. Mechanical tests

Tensile tests of the fibres were done at room temperature at a constant strain rate (50 μm/mn). Uniaxial tension tests used a 500 N load cell. The fibres were introduced inside metallic tube and fixed with glue.

Single-fibre push-out tests were performed on the SiC/SiC minicomposite specimen test using a nanoindenter (Nanotest from MicroMaterial Ltd.) to measure the intensity of the fibre/matrix bond and the interfacial shear stress. The samples were observed using SEM to check if the fibres are correctly loaded and the absence of damage on the fibres and matrix during the tests.

3. Results and discussion

Bulk and surface characterizations were performed on HNS and TSA3. The results are discussed in relation with the mechanical measurements of the SiC fibres and SiC-based composites.

3.1. Diameter distribution of the SiC fibres

The fibre diameter histograms for the three types of fibres (HNS (1), HNS (2), TSA3) are represented in Fig. 1. The average diameter of HNS fibres (around 13.0 μm) is much larger than the one of TSA3 fibre (7.0 μm). This is not surprising since it is known that the fibre diameter is strongly affected by the spinning step and the nature of the precursor. An important diameter dispersion is also observed inside a tow which can be related to the presence of imperfections.

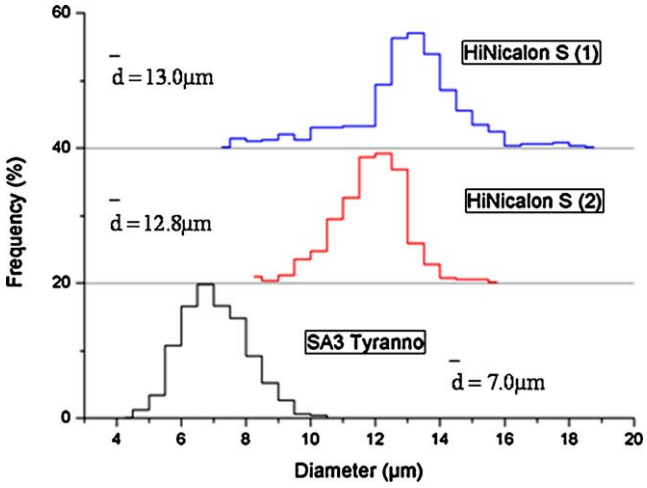

Fig. 1. Histograms of Hi-Nicalon S and SA3 Tyranno average diameter.

3.2. Mechanical properties of SiC fibres

The mechanical characteristics of the HNS and TSA3 tows/fibres are reported in Table 1. The values of the Young's modulus, ultimate failure and tensile strength for both fibres are close. It must be noted that the tensile strength of both fibres is higher than that of the previous generation of SiC fibres.[14–16] This improvement can be attributed to process modifications which reduce the presence of defects (surface imperfections, flaws, internal inclusions) and the amount of free carbon.[17,18]

The strength of the composite depends not only on the strength of the fibre reinforcement but also on the fibre strength distribution. The statistical variability of the fibre tensile strength is now commonly reported in terms of Weibull modulus (m) which is a parameter used to describe this strength distribution.[10,19] Therefore, the m modulus and the tensile strength will be also dependent on the flaws or imperfections (defects) of the fibres.

The stress–strain curves of the minicomposites reinforced with HNS and TSA3 fibres at room temperature are reported in Fig. 2. Both composites show a typical behaviour.[11,13,20]

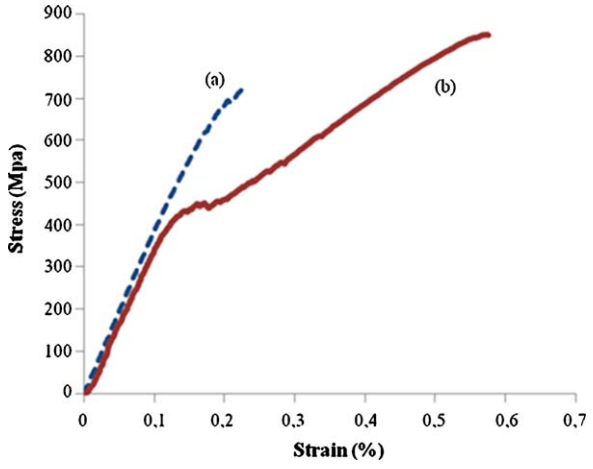

Fig. 2. Typical behaviour obtained with (a) the SA3 Tyranno and (b) Hi-Nicalon S reinforced SiC/SiC minicomposites.

Table 1
Main mechanical characteristics of fibre tows (rupture strength F_r, Young's modulus E, strain-to-failure ε_r, proportional limit strength σ_1, strength σ_{tow}, fraction of fibres broken prior to loading γ, critical fraction of individual fibre break α_c, fibre Weibull modulus m and scale factor σ_0).[11]

Fibre	F_r (N)	E (Gpa)	ε_r (%)	σ_{tow} (Mpa)	α_c (%)	γ (%)	σ_1 (Mpa)	m	σ_0 (Mpa)
HNS (1) (2)	120	319	0.73	2477	12.3	14.1	1338	6.4	1289
TSA3	118	312	0.68	2412	6.0	19.5	1231	8.2	1353

A difference in the tensile strain is however observed since the failure strain of the composites reinforced by TSA3 fibres is smaller ($\varepsilon_r \sim 0.3\%$) than the one of the HNS reinforced composites ($\varepsilon_r \sim 0.7\%$).

Since both fibres exhibit similar mechanical characteristics, the different mechanical behaviour observed can be attributed to the F/M interfacial coupling. The mechanical properties of the F/M interface were measured thanks the push-out test which emerged as the standard test.[21–23] Single-fibre push-out tests were carried out on the SiC/SiC minicomposites. The analysis of the load–displacement curves gives access to the strength (F_g) that must be applied to the fibre to extract itself in totality and hence to disrupt the interfacial bonding. The measurement of F_g allows to calculate the interfacial shear strength (τ_s) using the following equation (Eq. (1)):

$$\tau_s = \frac{F_g}{2\pi . r_f . l_f} \quad (1)$$

where r_f is the fibre radius and l_f is the fibre length.

As seen in Table 2, the interfacial shear strength is much higher for the TSA3-minicomposites. It indicates that the F/M bonding is stronger when the composite is reinforced with TSA3 fibre compared to HNS fibre as already suggested by the strain failure value. Since both composites only differ by the nature of their reinforced fibres, the difference in the strength of the F/M interfacial bonding can be related to the fibre/interphase bonding linked to the fibre surface properties.

To better understand the influence of surface properties, both types of fibres will be analyzed in terms of phase composition, structure, surface roughness and surface chemistry as described in the following section.

3.3. Bulk characterization of the SiC fibres

3.3.1. Phase composition and structure

XRD patterns of the HNS and TSA3 are shown in Fig. 3. The main phase detected for the three fibres corresponds to β-SiC (marked with a star) with five peak positions at $2\theta = 35.7°$, 41.5°, 60.2°, 71.8°, and 71.8° which are attributed to the (1 1 1), (2 0 0), (2 2 0), (3 1 1) and (2 2 2) reflections, respectively. The other phase, corresponding to α-SiC structure, is assigned to a weak diffraction peak at $2\theta = 33.6°$ due to the presence of stacking faults in β-SiC structure. The better crystallinity of TSA3 fibre results from the higher sintering temperature applied during the process.[24]

Table 2
Interfacial shear strength obtained by push-out tests on SiC/SiC composites using HNS and TSA3 fibres.

Material	HNS/SiC	TSA3/SiC
τ_s (MPa)	15	109

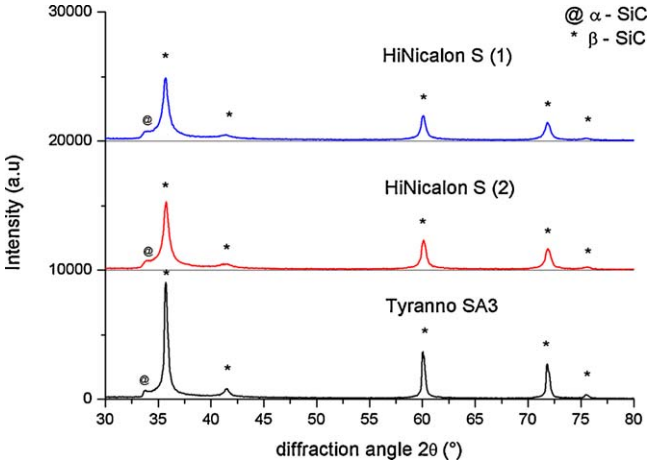

Fig. 3. X-ray diffractograms of the Hi-Nicalon S (1), Hi-Nicalon S (2) and SA3 Tyranno fibre.

The elemental composition and the C/Si ratio determined by ICP-AES are reported in Table 3 for both fibres. For the SA3 fibres, the Al composition was found equal to 0.13 at.%. Whatever the type of fibres, the C/Si ratio is slightly higher than 1 indicating that the fibres contain free carbon.

The Raman spectra of the two types of fibres are represented in Fig. 4. Two intense peaks can be observed at about 1350 and 1600 cm^{-1} which are attributed to sp^3 and sp^2 bonded carbon, respectively.[25] The peak at 1350 cm^{-1} is associated to the

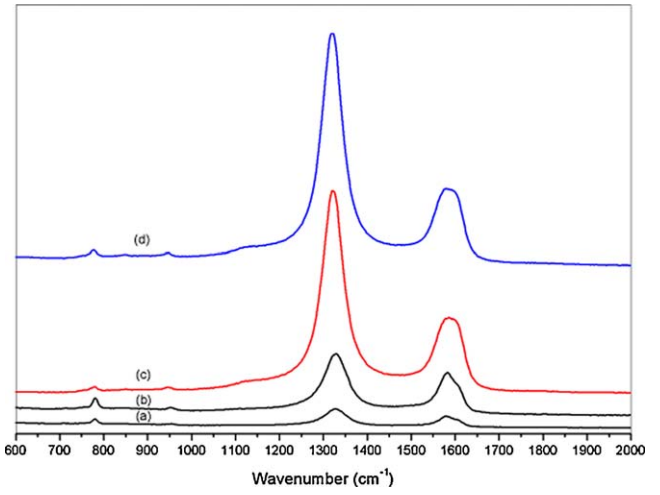

Fig. 4. Raman spectra of the SA3 Tyranno edge (a) and core (b), Hi-Nicalon S (1) core (c) and Hi-Nicalon S (2) core (d).

Table 3
Elementary chemical analysis by ICP-AES.

Fibre	Hi-Nicalon S (1)	Hi-Nicalon S (2)	Tyranno SA3
Chemical analysis (W%)			
Si	66.94	66.55	66.51
C	31.74	31.35	31.91
O	1.32	1.85	1.43
Al	–	–	0.13
C/Si (at.%)	1.10	1.13	1.12
Chemical formula	$SiC_{1.10}O_{0.016}$	$SiC_{1.13}O_{0.022}$	$SiC_{1.12}O_{0.017}Al_{0.0009}$

defects at the graphite edge plane whereas the peak at 1600 cm^{-1} is generally attributed to the E_{2g} symmetry (G peak) vibration mode in a graphite single crystal. Raman analysis was performed along the fibre axis from the edge to the core (Fig. 4). It can be observed that the amount of free carbon increases near the fibre core for the TSA3 sample. On the contrary, no significant change is observed between the core and the edge fibre for the HNS sample. For all samples, two peaks appear at 790 and 970 cm^{-1} corresponding to β-SiC. Raman analysis confirms that both fibres contain a fraction of low structural organized free carbon. For the TSA3 fibre, there is a concentration gradient of free carbon from the edge to the core towards the fibre.

The concentration profiles of C, Si, Al and free carbon along the fibre diameter was also determined by EPMA analysis and the results are reported in Figs. 5 and 6. For both types of fibres, the C/Si ratio is higher than 1 along the whole fibre diameter confirming the presence of free carbon as already indicated by ICP-AES and Raman. As seen in Fig. 5(a) and (b) for the HNS fibre, the atomic composition remains constant along the fibre diameter with a very low oxygen atomic concentration (∼1 at.%). In the case of the TSA3 fibre, it can be observed that the C concentration increases while the Si concentration decreases from the edge to the core of the fibre. This is related to the concentration of free carbon which is much higher in the core of the TSA3 fibre (∼8 at.% in the edge and ∼17 at.% in the core) as indicated in Fig. 6. It can be noted in the same figure that the free carbon concentration remains constant along the fibres axis for the HNS fibres with a value close to the one measured at the edge of the TSA3 fibre. Therefore, the EPMA measurements confirm the results obtained by the elemental composition and Raman analysis, i.e., the presence of free carbon in the SiC fibres

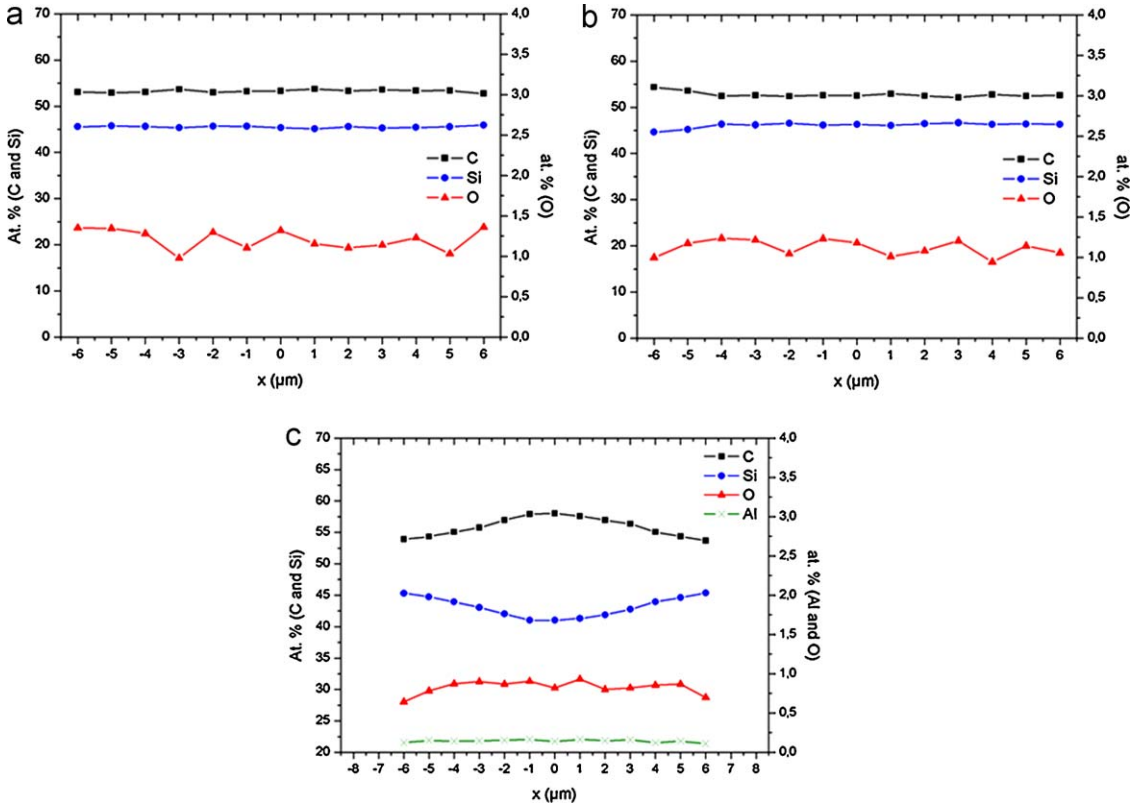

Fig. 5. C Si and O atomic concentration along the diameter of Hi-Nicalon S (1) (a) and Hi-Nicalon S (2) (b) and C, Si, O and Al atomique concentration along the diameter of SA3 Tyranno fibre (c) obtained by EPMA.

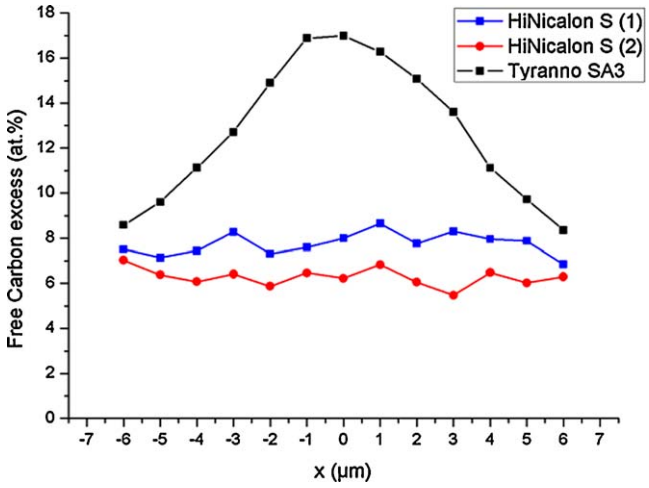

Fig. 6. Atomic concentration of free carbon along the diameter of the Hi-Nicalon S and SA3 Tyranno fibre.

and the existence of a composition gradiant for the TSA3 fibres with a much higher concentration of carbon in the fibre core.[26]

For the HNS fibres, the free carbon is formed during the electron beam curing step leading to the polymerization of the organosilicate precursor.[27] In the case of the TSA3 fibre, it arises from the thermal decomposition and sintering of Si–Al–C–O precursor. The analysis points out the existence of a concentration gradient along the fibre axis. This gradiant results from the reactions occurring during the thermal treatment and the presence of sintering aids (metal additive like aluminum). Indeed, the thermal decomposition and sintering of Si–Al–C–O fibre precursor lead to the formation of SiO and CO gases which diffuse from the core to the edge of the fibre. It is assumed that the sintered silicon carbide first created at the surface become thick and tight enough to slow down the gases diffusion (and hence modify the CO and SiO partial pressures). As a consequence, a skin/core effect takes place due to the fact that oxygen can be preferentially removed as SiO and free carbon is formed in the core of fibre.[28–31] As underlined by our analysis, this free carbon corresponds to a pyrolytic type carbon. As mentioned in the literature, this pyrolytic carbon can surrounded the SiC crystallites[32] or be present as microcrystallites inclusions dispersed into the SiO_xC_y matrix[33–36] or be a sp^3 bonded carbon which is not linked to silicium in the structural units [C–(C_x–Si_y)].

3.4. Surface characterization of the SiC fibres

The fibre surface was characterized by AFM and XPS in order to get information on the surface roughness and surface chemistry, respectively. At our knowledge, no data are available in the literature concerning the study of the surface chemistry of HNS and TSA3 fibres.

3.4.1. Surface roughness

SEM images of HNS (1), HNS (2) and TSA3 are shown in Fig. 7. It can be observed (Fig. 7e and f) that the surface of TSA3 fibre is much rougher. This roughness was quantified by AFM in tapping mode. The AFM images of the fibre surface are reported in Fig. 8. Two roughness factors (R_{max} and R_{RMS}) were determined from the AFM image of the fibre surface reported in Fig. 8. The values of R_{max} and R_{RMS} summarized in Table 4 correspond to the maximum amplitude determinated in the analyzed surface (500 nm × 500 nm) and to the quadratic mean amplitude, respectively. It can be noted that the R_{RMS} value is three times higher for TSA3 confirming the SEM analysis. R_{RMS} values of the two HNS batches are close. The R_{max} values indicate that the surface amplitude roughness of TSA3 fibres is twice larger than that of the HNS fibre. The surface roughness discrepancy between the two types of fibres is significant enough to modify the interfacial shear strength (τ_s). Shear stress, determinated by the push-out test (Eq. (1)), is also linked to the surface roughness as explained below. In fact τ_s can be calculated as follows:

$$\tau_s = -\mu\sigma_T \quad (2)$$

where μ is the friction coefficient and σ_T is the residual stresses.

Furthermore, the radial residual stresses (σ_T) can be determined as follows (Eq. (3)).

$$\sigma_T = \sigma_{th} + \sigma_R \quad (3)$$

where σ_R corresponds to the radial residual stress induced by fibre surface roughness and σ_{th} is the thermally radial residual stress which results from the mismatch in the thermal expansion coefficient between the fibre and the matrix. The values of σ_{th} in radial direction for both types of fibres are reported in Table 5. They were determined as explained in our previous paper by considering a single fibre and concentrically cylinders of fibre and matrix.[13]

It can be noted that the values of σ_{th} are close for both fibres. As a consequence, σ_T in radial direction will mainly depend on σ_R which is related to the surface roughness according to the following equation:

$$\sigma_R = \left(\frac{A}{r_f}\right)\frac{E_m E_f}{E_f(1+\nu_m)+E_m(1-\nu_f)} \quad \text{with} \quad A = 2 \times R_{RMS} \quad (4)$$

where A is the amplitude of lateral displacements induced by the surface roughness quantified through the RMS parameter,

Table 4
Surface roughness of silicon carbide fibres.

Fibre	Hi-Nicalon S (1)	Hi-Nicalon S (2)	Tyranno SA3
R_{RMS} (nm)	3.0	3.7	9.0
R_{max} (nm)	25.0	25.4	56.1

Table 5
Radial residual stresses induced by: thermally radial residual stresses (σ_{th}),[13] fibres surface roughness (σ_R) described by Eq. (4) and computation of radial residual stresses ($\sigma_T = \sigma_{th} + \sigma_R$).

Fibre	Hi-Nicalon S (1)	Hi-Nicalon S (2)	Tyranno SA3
σ_{th} (Mpa)	−200	−200	−130
σ_R (Mpa)	184	233	1020
σ_T (Mpa)	−16	33	890

−, tensile.
+, compressive.

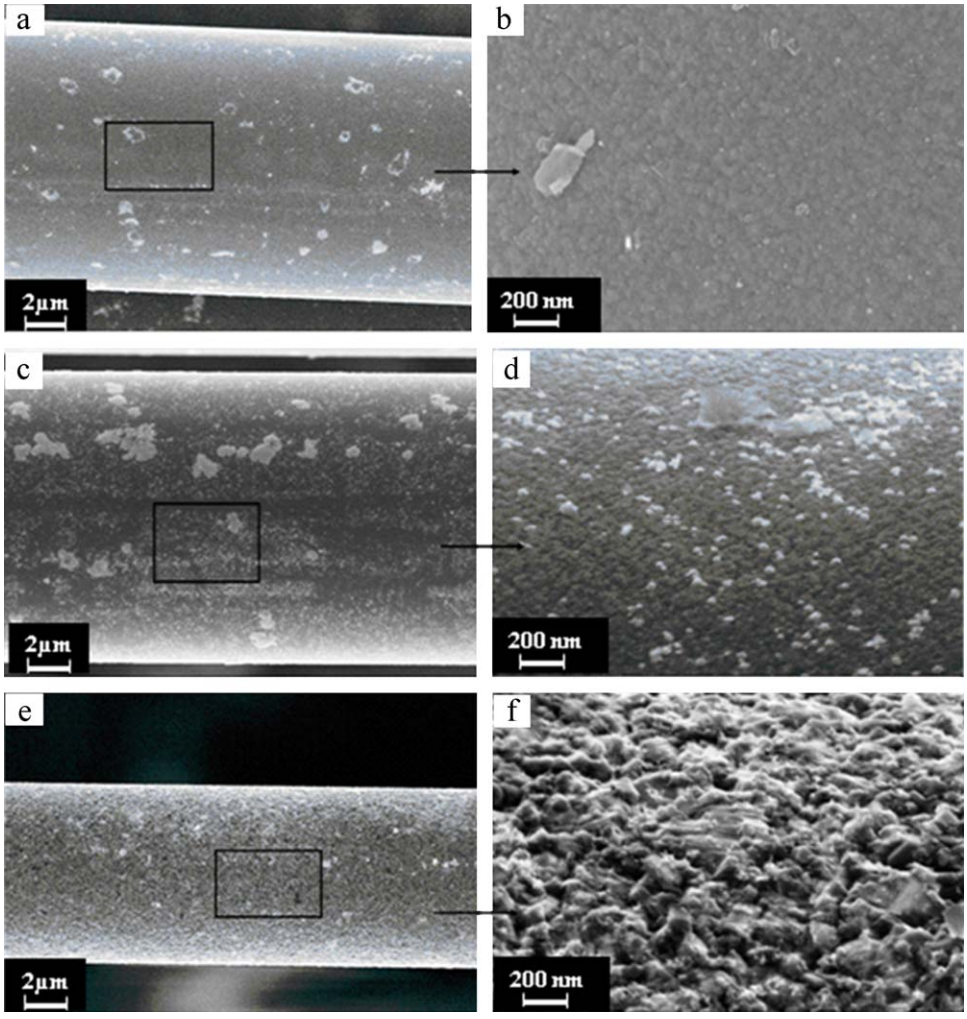

Fig. 7. SEM images of HNS (1) (a and b), HNS (2) (c and d) and TSA3 (e and f).

r_f the fibre radius, ν_f and ν_m the Poisson's modulus of fibre and matrix and E_m and E_f, the Young's modulus of the matrix and the fibre, respectively. As indicated in Table 5, the values of σ_{th} and σ_R compensate themself (compressive and tensile radial stresses are close) for the HNS-based minicomposite leading to a low value of the radial residual stresses (σ_T). On the contrary, the TSA3 minicomposite exhibits a much higher radial residual stresses due to the high value of the compressive radial stresses induced by the important surface roughness of the TSA3 fibre. As a consequence the τ_s discrepancy observed between the two types of fibres can be attributed to the surface roughness difference.

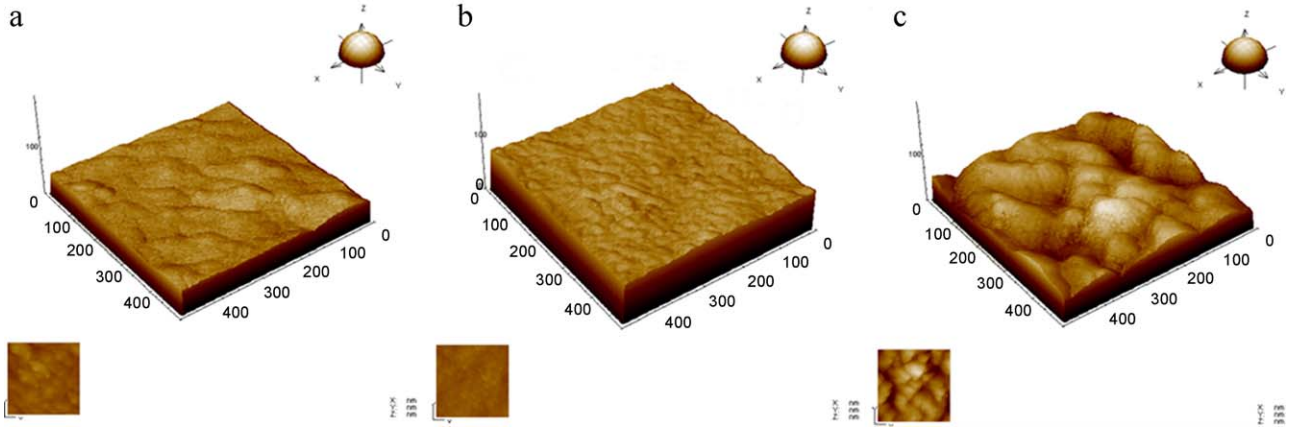

Fig. 8. AFM images of HNS (1) (a), HNS (2) and TSA3 (c) fibres.

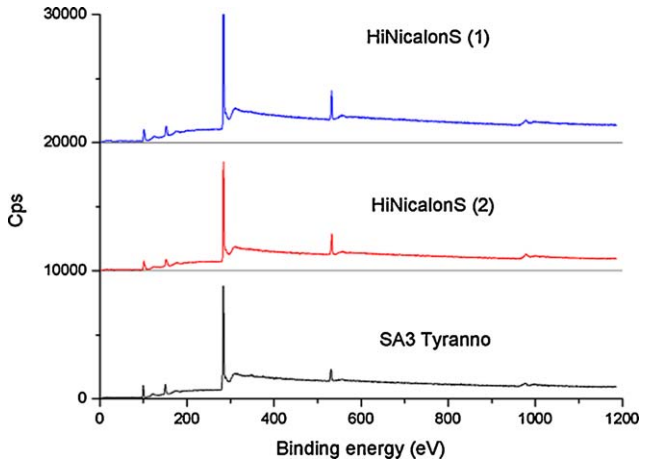

Fig. 9. Survey XPS spectra of Hi-Nicalon S (1), Hi-Nicalon S (2) and SA3 Tyranno fibres.

These results confirm that the surface roughness is one of the main parameter which controls the interfacial shear stress and consequently the F/M coupling.

Beside the roughness, the surface chemistry of the fibres was also analyzed since it can also play a crucial role on the nature of the F/M coupling.

3.4.2. Surface chemistry of the SiC fibres

The knowledge of the surface chemistry within the first nanometers is essential to predict the F/M cohesion. As shown in previous papers,[24] AES analysis enables to follow the evolution of the atomic concentration (C, Si, O and Al) in depth. A previous work indicates that the surface of both types of fibres (HNS and TSA3) is mainly constituted of free carbon (~65 at.% in the first 10 nm). It was also found that the C concentration decreases within 10–80 nm in depth whereas the silicon content increases. On the contrary, concentrations of Al and O remain almost constant. Two drawbacks of the AES analysis can be underlined: the quantitative analysis which is not reliable in the first ten nanometers and the irradiation during the analysis which modify the surface. To overcome these drawbacks, XPS analysis was performed. The survey XPS spectra are represented in Fig. 9 and the atomic concentration of C, O and Si deduced from the spectra analysis is summarized in Table 6. The survey analysis confirms that the surface fibre is mainly composed of carbon (~84%) whatever the fibres type. Elements such as silicon and oxygen are also clearly present but in much lower proportions. To identify the type of chemical bonds, high resolution spectra were recorded and fitted as explained in the experimental part using the fitting parameters given in Table 7 (Fig. 10). The C1s spectrum was fitted with eight components and the O1s with four components. In the Si2p spectra, the spin-orbit splitting was used, taking the 2p1/2 and 2p3/2 peak separation energy of 0.6 eV and a peak intensity ratio of 1/2.[37] Consequently, the Si2p peak was fitted with ten contributions.

Resulting data of the high resolution spectra fitted for HNS (1), (2) and TSA3 fibres are summarized in Table 8. Sp^2 bonded carbon is mainly present on the surface of HNS and TSA3 fibres. A small proportion of aliphatic carbon is observed for the three batches of fibres. The presence of free carbon at the surface can result from the elaboration process of HNS and TSA3 fibres and/or from the removal of the sizing. The decomposition of the Si2p spectra reveals that SiC, SiO_xC_y and SiO_2 are also present on the fibre surface (Table 8). Their atomic concentration remains however low compared to the carbon. The TSA3

Table 6
XPS qualitative analysis of Hi-Nicalon S (1), Hi-Nicalon S (2) and SA3 Tyranno fibre.

Fibre type	C1s (at.%)	O1s (at.%)	Si2p (at.%)
Hi-Nicalon S (1)	83.9	5.6	10.6
Hi-Nicalon S (2)	83.1	5.8	11.2
Tyranno SA3	84.3	4.1	11.6

Table 7
Fitting parameters of the C1s, Si2p and O1s peaks obtained from SiC fibres.

Item	Functional group	Binding energy (eV)	Ref.
C1s	C–Si	283.3	41
	SiO_xC_y	283.7	42
	Csp_2	284.3	43,44
	Csp_3	284.9	45
	C–CO	285.5	46
	C–O	286.2	47
	C=O	287.4	47
	COOR	288.4	47,48
Si2p	Si–C	99.5–100.6	42
	$SiOC_3$	100.2–3	42
	SiO_2C_2	101.2–6	42
	SiO_3C	102.1–2	42
	SiO_2	102.5–103	42

Table 8
Results of high resolution spectra fitted for HNS (1), HNS (2) and TSA3 fibres.

Fibre	Hi-Nicalon S (1)	Hi-Nicalon S (2)	Tyranno SA3
Components			
C1s (%)			
C–Si (1)	7.3	5.2	8.2
Csp_2 (2)	71.5	67.4	68.7
Csp_3 (3)	12.6	16.0	16.0
C–CO (4)	0.8	0.2	0.6
C–O (5)	0.8	0.7	0.2
SiO_xC_y (6)	2.5	3.7	1.7
C=O (7)	0.7	1.8	1.7
COOR (8)	0.8	0.2	0.6
Si2p (%)			
Si-C3/2 (1′)	31.7	29.8	45.2
Si-C1/2 (2′)	31.7	29.8	45.2
$SiOC_3$3/2 (3′)	0	0.3	0.1
$SiOC_3$1/2 (4′)	0	0.3	0.1
$SiO_2C_2$3/2 (5′)	4.5	9.8	3.5
$SiO_2C_2$1/2 (6′)	4.5	9.8	3.5
SiO_3C3/2 (7′)	3.2	0.5	0.8
SiO_3C1/2 (8′)	3.2	0.5	0.8
$SiO_2$3/2 (9′)	10.5	9.6	0.5
$SiO_2$1/2 (10′)	10.5	9.6	0.5

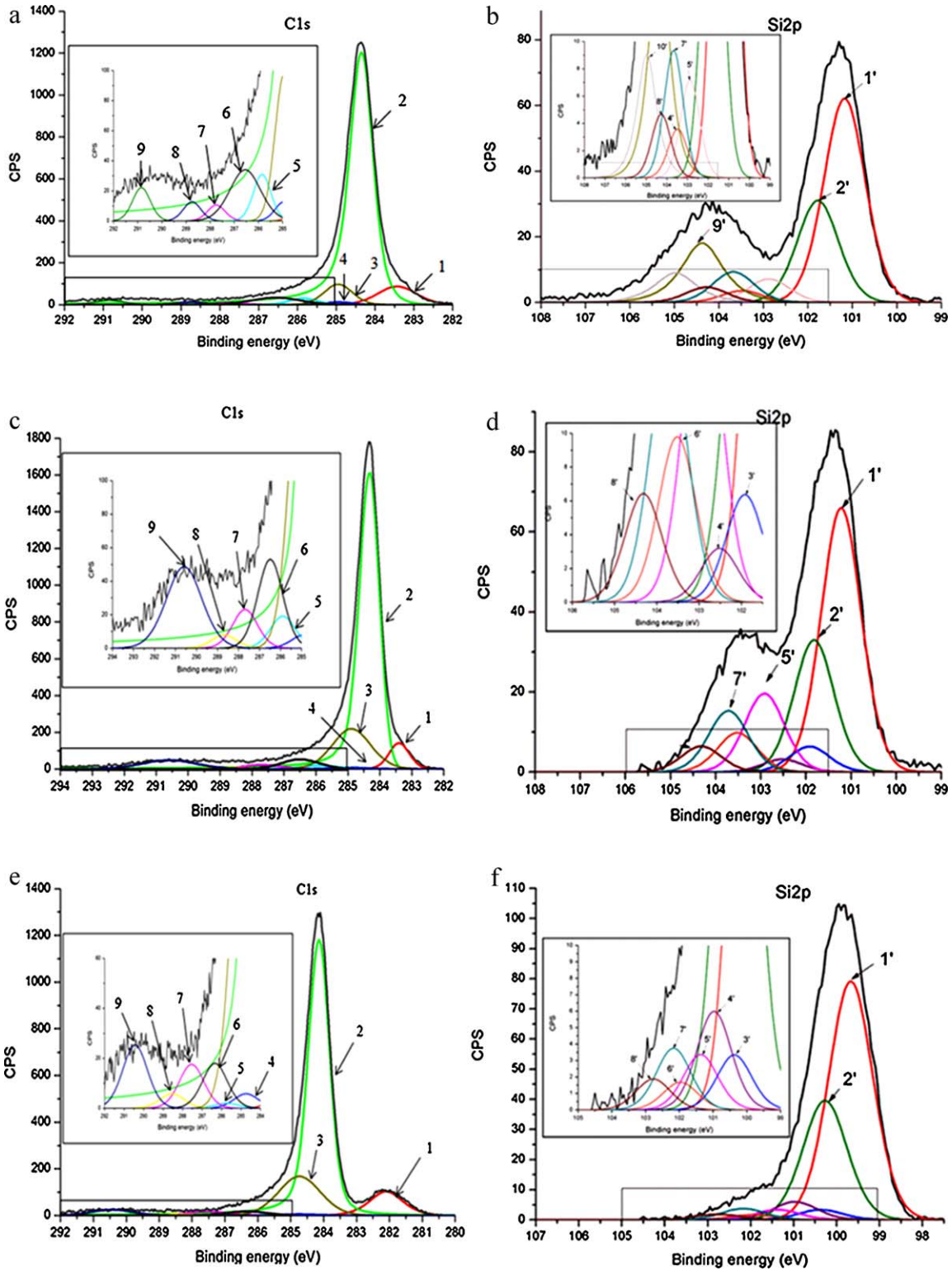

Fig. 10. High-resolution fitted C1s and Si2p of the Hi-Nicalon S (1) (a and b), Hi-Nicalon S (2) (c and d) and SA3 Tyranno (e and f) fibres.

surface is mainly composed of SiC; the fraction of SiO_2 being negligeable. On the contrary, the SiO_2 fraction is much higher in the case of the HNS fibre. This difference in the surface composition can be related to the fabrication process. In the case of the HNS fibre, the last heat treatment temperature is too low to completely decompose the SiO_xC_y compound and to promote the carbothermal reaction to reduce SiO_2 into SiC. The presence of SiC and SiO_2 is significant enough to modify the nature of the fibre/matrix interphase bond and consequently the mechanical properties. SiC reinforces the F/M bond whereas silica is known to weaken this F/M interface.[38,39] Oxide phases could be subject to strong changes under irradiation. Although, we believed that

this phase has no impact on the mechanical behaviour of SiC/SiC composites under irradiation environment since the amount of such oxide phases remains low compared to the other phase present on the fibre surface.[40] Due to the presence of SiC and the lack of SiO_2, the F/M interface for the minicomposite reinforced with TSA3 fibres will be stronger compared to the HNS-based composite. This could explain the more brittle behaviour of the TSA3 based composite.

The experimental results point out that the quality of the F/M interphase responsible of the mechanical properties will depend on the fibre surface roughness and fibre surface chemistry.

4. Conclusion

The aim of this work was to identify the characteristics of the SiC fibres influencing the F/M bonding and hence the mechanical properties of the corresponding reinforced minicomposites. Two types of SiC fibres were analyzed (TSA3 and HNS). For the HNS fibres, the analysis was carried out on two batches. No significant differences can be observed between the two batches indicating that the HNS fibres can be fabricated in a homogeneous way. As highlighted by the experimental results, the mechanical behaviour of the minicomposite is correlated to the surface roughness and surface chemistry of the SiC fibres. These both parameters were quantitatively determined by AFM and XPS. The analysis points out that the TSA3 and HNS fibres display different surface characteristics. Contrary to the HNS fibres, TSA3 has a granular and rough surface which leads to an increase of the residual stress and consequently the interfacial shear strength. Although the surface of both fibres is mainly composed by sp^2 bonded carbon, SiC, SiO_xC_y and SiO_2, the amounts of oxide and carbide differ between the HNS and TSA3 fibres. As a result, the F/M bonding will be stronger in the case of the TSA3-based minicomposite explaining the more brittle behaviour. Therefore, this work clearly points out that the strength of the F/M interfacial bonding is controlled by the surface roughness and surface chemistry of SiC fibres. Although TSA3 fibre is more attractive for nuclear application due to its better thermal stability, the mechanical behaviour of composite reinforced by this fibre is brittle. The improvement of the mechanical behaviour of the TSA3-reinforced minicomposite must go through the modification of the fibre/matrix bonding (fibre surface roughness and/or extreme surface chemistry).

Acknowledgements

The authors are very grateful to P. Bonnaillie for his help in SEM images, P. Fioux for XPS analyses and S. Gree for Raman spectroscopy results.

References

1. Brunel L, Chauvin N, Mizuno T, Pauchon MA, Somers J. The generation IV project GFR fuel and other core materials. In: *GIF symposium – GEN IV international forum, 2009*. 2009. p. 135–41.
2. Jones RH, Giancarli L, Hasegawa A, Katoh Y, Kohyama A, Riccardi B, et al. Promise and challenges of SiCf/SiC composites for fusion energy applications. *Journal of Nuclear Materials* 2002;**307**:1057–72.
3. Katoh Y, Kohyama A, Hinoki T, Snead LL. Progress in SiC-based ceramic composites for fusion applications. *Fusion Science and Technology* 2003;**44**(1):155–62.
4. Snead LL, Katoh Y, Kohyama A, Bailey JL, Vaughn NL, Lowden RA. Evaluation of neutron irradiated near-stoichiometric silicon carbide fiber composites. *Journal of Nuclear Materials* 2000;**283**:551–5.
5. Yamada R, Taguchi T, Igawa N. Mechanical and thermal properties of 2D and 3D SiC/SiC composites. *Journal of Nuclear Materials* 2000;**283**:574–8.
6. Hinoki T, Snead LL, Katoh Y, Hasegawa A, Nozawa T, Kohyama A. The effect of high dose/high temperature irradiation on high purity fibers and their silicon carbide composites. *Journal of Nuclear Materials* 2002;**307**:1157–62.
7. Katoh Y, Nozawa T, Snead LL, Hinoki T. Effect of neutron irradiation on tensile properties of unidirectional silicon carbide composites. *Journal of Nuclear Materials* 2007;**367**:774–9.
8. Katoh Y, Snead LL, Nozawa T, Kondo S, Busby JT. Thermophysical and mechanical properties of near-stoichiometric fiber CVI SiC/SiC composites after neutron irradiation at elevated temperatures. *Journal of Nuclear Materials* 2010;**403**(1–3):48–61.
9. Bertrand S, Forio P, Pailler R, Lamon J. Hi-Nicalon/SiC minicomposites with (pyrocarbon/SiC) (n) nanoscale multilayered interphases. *Journal of the American Ceramic Society* 1999;**82**(9):2465–73.
10. Lissart N, Lamon J. Damage and failure in ceramic matrix minicomposites: experimental study and model. *Acta Materialia* 1997;**45**(3):1025–44.
11. Sauder C, Brusson A, Lamon J. Mechanical properties of Hi-NicalonS and SA3 fiber reinforced SiC/SiC minicomposites. *Ceramic Engineering and Science Proceedings* 2008;**29**:91–100.
12. Hasegawa A, Kohyama A, Jones RH, Snead LL, Riccardi B, Fenici P. Critical issues and current status of SiC/SiC composites for fusion. *Journal of Nuclear Materials* 2000;**283**(December):128–37.
13. Sauder C, Brusson A, Lamon J. Influence of interface characteristics on the mechanical properties of Hi-Nicalon and SA3 fiber reinforced SiC/SiC minicomposites. *International Journal of Applied Ceramic Technology* 2010;**7**(3):291–303.
14. Ishikawa T, Kohtoku Y, Kumagawa K, Yamamura T, Nagasawa T. High-strength alkali-resistant sintered SiC fibre stable to 2200 degrees C. *Nature* 1998;**391**(6669):773–5.
15. Kumagawa K, Yamaoka H, Shibuya M, Yamamura T. Fabrication and mechanical properties of new improved Si–M–C–(O) Tyranno fiber. 22nd annual conference on composites. *Advanced Ceramics, Materials, and Structures A* 1998;**19**(3):65–72.
16. Nakayasu T, Sato M, Yamamura T, Okamura K, Katoh Y, Kohyama A. Recent advancement of Tyranno/SiC composites R&D. *Ceramic Engineering and Science Proceedings* 1999;**20**(4):301–8.
17. Chollon G, Pailler R, Naslain R, Laanani F, Monthioux M, Olry P. Thermal stability of a PCS-derived SiC fibre with a low oxygen content (Hi-Nicalon). *Journal of Materials Science* 1997;**32**(2):327–47.
18. Mea T. Properties of stoichiometric silicon carbide fibre derived from PCS. *Ceramic Engineering and Science Proceedings* 1994;**15**(4):133–41.
19. Morimoto T, Yamamoto K, Ogihara S. Strength improvement on an imaginary SiC fiber of ideal diameter and reduced internal defects estimated from the Weibull scaling of Tyranno ZMI fiber. *JSME International Journal Series A: Solid Mechanics and Material Engineering* 2006;**49**(1):15–9.
20. Lamon J, Rebillat F, Evans AG. Microcomposite procedure for evaluating the interface properties of ceramic–matrix composites. *Journal of the American Ceramic Society* 1995;**78**(2):401–5.
21. Chandra N, Ghonem H. Interfacial mechanics of push-out tests: theory and experiments. *Composites Part A: Applied Science and Manufacturing* 2001;**32**(3–4):575–84.
22. Ho KKC, Kalinka G, Tran MQ, Polyakova NV, Bismarck A. Fluorinated carbon fibres and their suitability as reinforcement for fluoropolymers. *Composites Science and Technology* 2007;**67**:2699–706.
23. Jouannigot S, Lamon J. Mesure de l'intensité de la liaison interfaciale fibre/matrice par essais de push-out/push-back, application aux composites carbone–carbone. *Matériaux & Techniques* 2008;**96**:115–20.
24. Yuxi Y, Xueyuan T, Xiaodong L. Characterization and microstructural evolution of SiC(OAl) fibers to SiC(Al) fibers derived from

aluminum-containing polycarbosilane. *Composites Science and Technology* 2008;**169**:7–703.
25. Karlin S, Colomban P. Raman study of the chemical and thermal degradation of as-received and sol–gel embedded Nicalon and Hi-Nicalon SiC fibres used in ceramic matrix composites. *Journal of Raman Spectroscopy* 1997;**28**(4):219–28.
26. Dong SM, Chollon G, Labrugere C, Lahaye M, Guette A, Bruneel JL, et al. Characterization of nearly stoichiometric SiC ceramic fibres. *Journal of Materials Science* 2001;**36**(10):2371–81.
27. Tazi Hemida A, Pailler R, Naslain R. Continuous SiC-based model monofilaments with a low free carbon content. 1. From the pyrolysis of a polycarbosilane precursor under an atmosphere of hydrogen. *Journal of Materials Science* 1997;**32**(May (9)):2359–66.
28. Bodet R, Jia N, Tressler RE. Microstructural instability and the resultant strength of Si–C–O (Nicalon) and Si–N–C–O (HPZ) fibres. *Journal of the European Ceramic Society* 1996;**16**(6):653–64.
29. Delverdier O, Monthioux M, Mocaer D, Pailler R. Thermal-behavior of polymer-derived ceramics. 1. Si–C and Si–C–O systems from both commercial and new polycarbosilane (PCS) precursors. *Journal of the European Ceramic Society* 1993;**12**(1):27–41.
30. Sawyer LC, Chen RT, Haimbach F, Harget PJ, Prack ER, Jaffe M. *Ceramic Engineering and Science Proceedings* 1986;**7**(7):914.
31. VixGuterl C, Ehrburger P. Effect of thermal treatment on the reactivity of SiC-based fibres. *Journal of Materials Science* 1996;**31**(20):5363–71.
32. Lipowitz J, Freeman HA, Chen RT, Prack ER. Composition and structure of ceramic fibers prepared from polymer precursors. *Advanced Ceramic Materials* 1987;**2**(2):121–8.
33. Bouillon E, Mocaer D, Villeneuve JF, Pailler R, Naslain R, Monthioux M, et al. Composition microstructure property relationships in ceramic monofilaments resulting from pyrolysis of a polycarbosilane precursor at 800 to 1400-degrees-C. *Journal of Materials Science* 1991;**26**(6):1517–30.
34. Laffon C, Flank AM, Lagarde P, Bouillon E. Study of the polymer to ceramic evolution induced by pyrolysis of organic precursor. *Physica B* 1989;**158**(1–3):229–30.
35. Maniette Y, Oberlin A. TEM characterization of some crude or air heat-treated SiC Nicalon fibers. *Journal of Materials Science* 1989;**24**(9):3361–70.
36. Yajima S, Okamura K, Tanaka J, Hayase T. High-temperature strengths of aluminum composite reinforced with continuous SiC fiber. *Journal of Materials Science* 1981;**16**(11):3033–8.
37. Socha RP, Laajalehto K, Nowak P. Oxidation of the silicon carbide surface in Watts' plating bath. *Surface and Interface Analysis* 2002;**34**(1):413–7.
38. Bertrand S, Forio P, Pailler R, Lamon J. Hi-Nicalon/SiC minicomposites with (Pyrocarbon/SiC)n nanoscale multilayered interphases. *Journal of American Ceramic Society* 1999;**82**(9):2465–73.
39. Bertrand S, Pailler R, Lamon J. Influence of strong fiber/coating interfaces on the mechanical behaviour and lifetime of Hi-Nicalon/(PyC/SiC)n/SiC minicomposites. *Journal of American Ceramic Society* 2001;**84**(4):787–94.
40. Ozawa K, Nozawa T, Katoh Y, Hinoki T, Kohyama A. Mechanical properties of advanced SiC/SiC composites after neutron irradiation. *Journal of Nuclear Materials* 2007;**367**:713–8.
41. Flores M, Fuenzalida V, Haberle P. Thermal effects in the size distribution of SiC nanodots on Si(111). *Physica Status Solidi A: Applications and Materials Science* 2005;**202**(10):1959–66.
42. Shimoda K, Park JS, Hinoki T, Kohyama A. Influence of surface structure of SiC nano-sized powder analyzed by X-ray photoelectron spectroscopy on basic powder characteristics. *Applied Surface Science* 2007;**253**:9450–6.
43. Bismarck A, Tahhan R, Springer J, Schulz A, Klapotke TM, Zell H. Influence of fluorination on the properties of carbon fibres. *Journal of Fluorine Chemistry* 1997;**84**(2):127–34.
44. Lohner T, Pongracz A, Khanh NQ, Krafcsik OH, Josepovits KV, Deak P. Comparative investigation of the Si/SiO_2 interface layer containing SiC crystallites using spectroscopic ellipsometry, ion beam analysis and XPS. *Physica Status Solidi C: Current Topics in Solid State Physics* 2008;**5**(5):1337–40.
45. Moravec TJ, Orent TW. Electron-spectroscopy of ion-beam and hydrocarbon plasma generated diamond-like carbon-film. *Journal of Vacuum Science & Technology* 1981;**18**(2):226–8.
46. Charlier J, Detalle V, Valin F, Bureau C, Lecayon G. Study of ultrathin polyamide-6,6 films on clean copper and platinum. *Journal of Vacuum Science & Technology A: Vacuum Surfaces and Films* 1997;**15**(2):353–64.
47. Socha RP, Laajalehto K, Nowak P. Influence of the surface properties of silicon carbide on the process of SiC particles codeposition with nickel. *Colloids and Surfaces A: Physicochemical and Engineering Aspects* 2002;**208**(1–3):267–75.
48. Vincent C, Vincent H, Berthet MP, Piquero T, Bouix J. ESCA characterization of boron and silicon carbide mixed layers deposited on HR and HM carbon fibres by RCVD: properties of the as-coated fibres. *Composites Part A: Applied Science and Manufacturing* 1996;**27**(5):365–77.